both values of ξ are sufficiently large. This *independence of ξ is only expected if the reduced potentials u at the same reduced distance r/R are compared in* two different polyelectrolyte systems *with the same value of* a^2C_e.

In a given polyelectrolyte system with $\xi \geq 2$, the counterions accumulate in the neighborhood of the polyion "surface", the fraction of accumulated counterions up to a given value of r/R increasing with ξ but decreasing with increasing values of a^2C_e. For high values of ξ ($\xi > 2$) and relatively high equivalent concentrations, more than 50% of all counterions will be found at a distance of a few nanometers from the distance of closest approach (for $|z_c| = 1$).

The scaling parameter χ of the Poisson–Boltzmann equation may be considered as a screening length as $(u)_{x>1}$ is always smaller than unity. Its value depends on a^2C_e, but if $\xi \geq 2.5$, it is practically independent of the charge parameter. It is of the same order of magnitude as, but somewhat larger than, the Debye length calculated taking into account only "noncondensed" counterions, i.e., $\rho_c^{(m)}/\xi$.

The fraction of accumulated counterions at $x = 1$ increases with ξ and decreases with a^2C_e. For $\xi > 2$ this fraction exceeds 60% and may become as high as 90% for large values of ξ and small values of a^2C_e (low concentrations and small value of a). The counterions within the screening length still occupy the smaller volume fraction of the cell volume. This distribution thus bears some resemblance with the "two-phase" model.

The same conclusions are valid for a system containing a weak polyelectrolyte, the charge parameter of which may be changed by titration with a strong low molar mass base of acid. In the course of the titration the radius of the cell R remains the same whatever the degree of charge of the polyelectrolyte. This means that R is no longer a function of ξ, and the ξ-dependence of u is determined only through $|B|$. Consequently, for constant a^2C_e, at any position in the cell including the polyion "surface" at a, the reduced potential u will level off with increasing ξ, thus displaying a condensation-like effect. This ξ-independence will, however, start at values considerably larger than $\xi = 1$ but depending only slightly on a^2C_e.

Elastic Constants of Hard and Soft Nematic Liquid Crystals

Broto Tjipto-Margo, Glenn T. Evans,*

Department of Chemistry, Oregon State University, Corvallis, Oregon 97331

Michael P. Allen,*

H. H. Wills Physics Laboratory, Royal Fort, Tyndall Avenue, Bristol BS8 1TL, England

and Daan Frenkel*

FOM Institute for Atomic and Molecular Physics, P. O. Box 41883, 1009 DB Amsterdam, The Netherlands
(Received: September 9, 1991)

The Frank elastic constants for a nematic liquid crystal have been calculated by computer simulations for a fluid of hard ellipsoids and by the Poniewierski–Stecki method for ellipsoids with and without an attractive square well. Required for the Poniewierski–Stecki method is the direct correlation function $c(1,2)$ and its dependence on the mutual molecular orientations. This was addressed using several models: the Parsons model, a two-term virial expansion, and the PY and HNC theories of Patey et al. In the Parsons model for $c(1,2)$, the derived Frank elastic constants for hard ellipsoids were in agreement with the Poniewierski–Holyst values for hard spherocylinders. However, the agreement with simulation values was less satisfactory, as the simulation values exceeded the Parsons model values and the discrepancy grew with increasing particle asymmetry. The Frank constants, derived using a hard-core potential with an exterior SW (convex peg in a round hole), were in fair agreement with experimental data on prolate and oblate molecules, at the expense of employing overly large-order parameters (characteristic of uniaxial hard particle models). Omitted long-range correlations in the $c(1,2)$, present even in the hard-body models, is suspected to be the cause of the discrepancy of the simulation and experimental Frank constants with those calculated on the basis of short-range models for $c(1,2)$.

I. Introduction

The Frank elastic constants of a liquid crystal are the "force constants" that dictate the change in the Helmholtz free energy of the nematic phase as the liquid crystal is bent, splayed, or twisted.[1] These macroscopic force constants, which are of technological importance (for the design of liquid-crystal displays), possess information on the microscopic anisotropic intermolecular forces in the liquid-crystalline phase. In the present work, we calculate the Frank constants for hard-particle systems and for hard particles encased in a spherical square well. Two approaches are taken: computer simulations for the hard-particle systems; and a method due to Poniewierski and Stecki (PS)[2] for both the hard- and soft-particle systems. Potential softness will be addressed in the context of a van der Waals model as this allows the density and temperature dependence of the Frank constants to be clearly displayed.

PS first derived an expression which related the Frank constants to integrals of the direct correlation function (or the dcf). In response to that work, several groups[3-6] have verified the PS finding and have derived the same results using a more direct density functional (DF) approach. Gelbart and Ben-Shaul[7] had provided an alternative (and equivalent) procedure for the calculation of

(1) See, e. g.: de Gennes, P.-G. *The Physics of Liquid Crystals*; Oxford University Press: Oxford, 1974. Chandrasekhar, S. *Liquid Crystals*; Cambridge University Press: Cambridge, 1977.

(2) Poniewierski, A.; Stecki, J. *Mol. Phys.* **1979**, *38*, 1931; *Phys. Rev.* **1982**, *A25*, 2368.
(3) Singh, Y. *Phys. Rev.* **1983**, *A30*, 583.
(4) Lipkin, M. D.; Rice, S. A.; Mohanty, U. *J. Chem. Phys.* **1985**, *82*, 472.
(5) Masters, A. J. *Mol. Phys.* **1985**, *56*, 887.,
(6) Somoza, A. M.; Tarazona, P. *Mol. Phys.* **1991**, *72*, 911.
(7) Gelbart, W. M.; Ben-Shaul, A. *J. Chem. Phys.* **1982**, *77*, 916.

0022-3654/92/2096-3942$03.00/0 © 1992 American Chemical Society

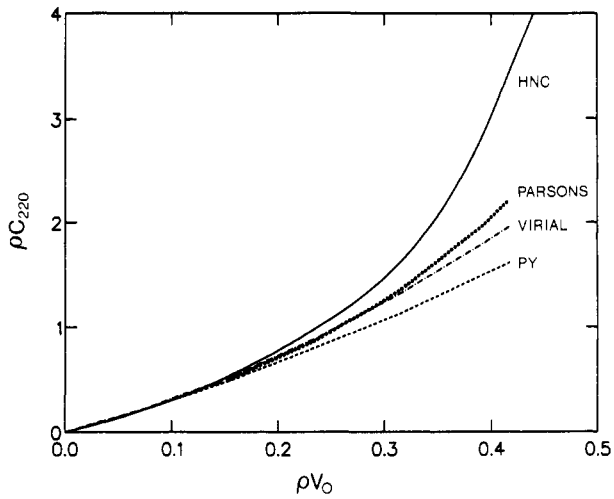

Figure 1. Comparison of the HNC, the Parsons model, two term virial model and PY representations of ρC_{220}.

the Frank constants, and it too involves integrals over the direct correlation function. As a consequent, the issue of a derivation of working expressions for the Frank constants has been rendered closed. What is still needed is an analysis of the adequacy of the PS theory to "explain" the simulation results and the experimental results on prolate and oblate molecules, and to that we now turn.

II. Theory

(1) Background. The Frank constants for uniaxial molecules are given by the following expression:[2-6]

$$\{K_i|i=1,2,3\} = \tfrac{1}{2}\rho^2 k_B T \int \mathrm{d}\mathbf{r}\, \mathrm{d}\Omega_1 \mathrm{d}\Omega_2\, c(1,2)\{r_x^2, r_y^2, r_z^2\} e_{1x} e_{2x} f'(\hat{\mathbf{e}}_1\cdot\hat{\mathbf{z}}) f'(\hat{\mathbf{e}}_2\cdot\hat{\mathbf{z}}) \quad (1)$$

Here the director axis is taken along $\hat{z}$ and accordingly K_1 is the Frank constant for splay, K_2 for twist, and K_3 for bend. Employed in eq 1 are ρ ($=N/V$) the density, $c(1,2)$ the two-particle dcf in the nematic phase, $\mathbf{r}$ the center-to-center vector of the 1,2 pair, e_{ix} the projection of the major axis of molecule i along the lab-fixed $\hat{\mathbf{x}}$ axis, Ω_i the molecular orientation angles, and $f(\hat{\mathbf{e}}_i\cdot\hat{\mathbf{z}})$ the orientational distribution function in the nematic phase. The prime on f is the derivative with respect to $\hat{\mathbf{e}}_i\cdot\hat{\mathbf{z}}$. Given an expression for $c(\mathbf{r},\hat{\mathbf{e}}_1,\hat{\mathbf{e}}_2)$ ($\equiv c(1,2)$), the determination of the Frank constants is an issue of integration.

To proceed with the calculation of the $\{K_i\}$, one must have an expression for the dcf, and to do this, consider Figure 1. Shown in Figure 1 is the variation of the second rank Legendre moment of $\rho c(1,2)$

$$\rho C_{220} = \rho \int \mathrm{d}\mathbf{r}\, \mathrm{d}\hat{\mathbf{e}}_1\, \mathrm{d}\hat{\mathbf{e}}_2\, c(1,2)\, P_2(\hat{\mathbf{e}}_1\cdot\hat{\mathbf{e}}_2) \quad (2)$$

for fluids of 3:1 hard uniaxial ellipsoids in various approximations. The HNC and PY curves were determined by Perera et al.[8] from the solutions of the appropriate integral equations. In the Parsons[9] model, the direct correlation function is approximated by

$$c(1,2) = \Phi_{12}(1 - \tfrac{3}{4}\rho^*)/(1-\rho^*)^2 \quad (3a)$$

where Φ_{ij} is the Mayer "f" bond and ρ^* is the packing fraction ($\rho^* = \rho v_0$, with v_0 the hard-core volume per particle). Explicitly, a Parsons model predicts that

$$\rho C_{220} = -2\rho(1 - \tfrac{3}{4}\rho^*)B_{2,2}/(1-\rho^*)^2 \quad (3b)$$

where $B_{2,2}$ is the second-rank Legendre expansion coefficient of the second virial coefficient given by eq 25 of ref 10. Finally, by the virial model we mean the B_2, B_3 Onsager theory[10] in which

$$c(1,2) = \Phi_{12} + \rho \int \mathrm{d}3\, \Phi_{12}\Phi_{23}\Phi_{13} \quad (4a)$$

$$\rho C_{220} = -2\rho B_{2,2} - 15^{1/2}\rho^2 B_3[2,2,0] \quad (4b)$$

Here $B_3[2,2,0]$ is the 2,2,0 expansion coefficient of the third virial coefficient, given numerically in Table III of ref 10.

The consequences of the findings shown in Figure 1 on the isotropic to nematic (I–N) transition are significant. From a bifurcation analysis of the I–N transition, one obtains an approximate stability[11-13] condition for the nematic phase, i.e., $\rho C_{220} > 5$. From this condition, one can assess the anisotropy of $c(1,2)$. Actually the quoted stability condition is too strong, as the transition usually takes place at somewhat lower densities. As seen from Figure 1, the PY derived values for ρC_{220} are considerably less than 5 over the whole density range and hence the PY theory for $c(1,2)$ does not predict an I–N transition. At the other extreme, the HNC values for ρC_{220} are too large as evidenced by an I–N transition density which occurs at a density roughly 30% below the simulation values. Between these two cases (over- and underestimating ρC_{220}) we find the Parsons and B_2, B_3 Onsager models.

The Onsager model for ρC_{220} has a weaker density dependence than the Parsons model and accordingly the I–N transition occurs at a higher density in the B_2, B_3 Onsager theory than in the Parsons theory (which overestimates the transition density obtained by computer simulation[14,15] by 10% for 3:1:1 ellipsoids). For 10:1:1 ellipsoids, the B_2, B_3 Onsager theory (by virtue of its exact three body correlations omitted from all current DFTs) is superior to the Parsons model. But as the molecules become less elongated, the convergence of the virial expansion is abated and approximate resummation techniques, such as those of the Parsons theory, become necessary. On the basis of the accuracy of the Parsons theory predictions of the transition densities (of the order of 10%), we infer that some of the anisotropy of $c(1,2)$ is portrayed accurately and hence the Parsons model will be used in the subsequent analysis of the Frank constants.

Of course, the actual $c(1,2)$ required in eq 1 pertains to the nematic phase and not the isotropic phase as we have assumed here. If the dcf is truly short ranged, then the calculated Frank constants will be insensitive to this distinction.

(2) van der Waals Model and the Convex Peg Potential. The van der Waals model for a liquid crystal[16-18] can be expressed in the language of the dcf, and the result is called a mean spherical approximation[19] (MSA). Consider the "convex peg in a round hole potential",[18,20] which exhibits infinite repulsion if the cores overlap (reside within the excluded volume $V_{ex}(\Omega_1,\Omega_2)$) and square-well (SW) attraction if the center-to-center distance is less than or equal to the sum of the largest semimajor axes, σ:

$$U(\mathbf{r},\Omega_1,\Omega_2) = \begin{cases} \infty & \mathbf{r} \in V_{ex}(\Omega_1,\Omega_2) \\ -\varepsilon & r \le \sigma, r \notin V_{ex} \end{cases} \quad (5)$$

When this potential is used in conjunction with the MSA, one obtains

$$c(\mathbf{r},\Omega_1,\Omega_2) = \begin{cases} \Phi_{12}\rho^\circ & \mathbf{r} \in V_{ex}(\Omega_1,\Omega_2) \\ \beta\varepsilon & r \le \sigma, \mathbf{r} \notin V_{ex} \end{cases} \quad (6a)$$

(8) Perera, A.; Patey, G. N.; Weis, J. J. *J. Chem. Phys.* **1988**, *89*, 6941.
(9) Parsons, J. D. *Phys. Rev.* **1979**, *A19*, 1225.
(10) Tjipto-Margo, B.; Evans, G. T. *J. Chem. Phys.* **1990**, *93*, 4254.
(11) Stecki, J.; Kloczkowski, A. *Mol. Phys.* **1981**, *42*, 51.
(12) Kayser, R. F.; Raveché, H. J. *Phys. Rev.* **1978**, *A17*, 2067.
(13) Perera, A.; Kusalik, P. G.; Patey, G. N. *Mol. Phys.* **1987**, *60*, 77; *J. Chem. Phys.* **1987**, *87*, 1295; *J. Chem. Phys.* **1988**, *89*, 5969. Perera, A.; Patey, G. N. *J. Chem. Phys.* **1988**, *89*, 5861.
(14) Frenkel, D.; Mulder, B. M. *Mol. Phys.* **1985**, *55*, 1171.
(15) Zarragoicoechea, G. J.; Levesque, D.; Weis, J. J. *Mol. Phys.*, preprint. From the results of these authors, $\rho_{NI}(N=256) \simeq 1.1\rho_{NI}(N=108)$, it would appear that the predictions of the transition density, based on the Parsons model for the direct correlation function, may be very accurate.
(16) Gelbart, W. M.; Barboy, B. *Acc. Chem. Res.* **1980**, *13*, 290.
(17) Cotter, M. A. In *The Molecular Physics of Liquid Crystals*; Luckhurst, G. R., Gray, G. W., Eds.; Academic Press: London, 1979.
(18) Tjipto-Margo, B.; Evans, G. T. *Mol. Phys.* **1991**, *74*, 85.
(19) See, e.g.: Hansen, J. P.; McDonald, I. R. *Theory of Simple Liquids*; 2nd ed.; Academic Press: London, 1986.
(20) Evans, D. R.; Evans, G. T.; Hoffman, D. K. *J. Chem. Phys.* **1991**, *94*, 8816. Evans, G. T.; Smith, E. B. *Mol. Phys.* **1991**, *74*, 79.

where the Parsons model has been used to represent the hard core and

$$\rho^\circ = (1 - {}^3/_4\rho^*)/(1 - \rho^*)^2 \tag{6b}$$

Equations 6a and 6b completely specify the dcf.

(3) Perturbation Expressions for the Frank Constants. For small order parameters, the Frank constants[7,21-23] can be expressed in a truncated power series:

$$K_i = \rho^2 k_B T\{\langle P_2\rangle^2 k_i^{22} + 2\langle P_2\rangle\langle P_4\rangle k_i^{24}\} \tag{7}$$

where $\langle P_n\rangle$ is the order parameter associated with the nth-rank Legendre polynomial. When the orientational distribution function is expanded as

$$f(\mathbf{e}\cdot\mathbf{z}) = (4\pi)^{-1}\sum_j (2j+1)P_j(\hat{\mathbf{e}}\cdot\hat{\mathbf{z}})\langle P_j\rangle \tag{8}$$

and eq 8 is inserted into eq 1, we obtain explicit integrals for each of the k_i^{mn}:

$$k_{i[1,3]}^{mn} = {}^1/_2(4\pi)^{-2}(2m+1)(2n+1)\times \int d\mathbf{r}\, d\Omega_1\, d\Omega_2\, c(1,2) r^2_{[j|x,y,z]} e_{1x}e_{2x}P'_m(\hat{\mathbf{e}}_1\cdot\hat{\mathbf{z}})P'_n(\hat{\mathbf{e}}_2\cdot\hat{\mathbf{z}}) \tag{9}$$

The integrations in eq 9 are performed over isotropic space, and hence only isotropic tensors (or rotational invariants constructed from r, $\mathbf{e}_1$, and $\mathbf{e}_2$) are needed to express $c(1,2)$. Cartesian rotational invariants have been derived[10] (see eq 38), and by means of these functions we can represent the $r^2_j e_{1x}\ldots P'_n(\hat{\mathbf{e}}_2\cdot\hat{\mathbf{z}})$ portion of the integrand in eq 9 by coordinate system independent functions. After some algebra we find that each of the k's can be written as a sume of just two rotational invariants integrated over $c(1,2)$:

$$k_{[1,2,3]}^{22} = {}^5/_2 C_{220}^{\prime} + (1/14)^{1/2}[-1,2,-1]C_{222}^{\prime} \tag{10a}$$

$$k_{[1,2,3]}^{24} = k_{[1,2,3]}^{42} = {}^{45}/_{16}C_{440}^{\prime} + (5/56)^{1/2}[-3,-1,4]C_{422}^{\prime} \tag{10b}$$

where we have used the notation

$$C_{jkm}^{\prime} = (4\pi)^{-2}\int d\mathbf{r}\, d\Omega_1\, d\Omega_2\, c(1,2) r^2(j,k,m) \tag{11}$$

with

$$(j,j,0) = P_j(x) \tag{12a}$$

$$(2,2,2) = (25/14)^{1/2}\{3(x^2+y^2+w^2) - 9xyw - 2\} \tag{12b}$$

$$(4,2,2) = {}^3/_8(10/7)^{1/2}\{35x^2y^2 - 5(x^2+y^2) - 20xyw + 2w^2 + 1\} \tag{12c}$$

$$x = \hat{\mathbf{e}}_1\cdot\hat{\mathbf{e}}_2 \qquad y = \hat{\mathbf{e}}_1\cdot\hat{\mathbf{r}} \qquad w = \hat{\mathbf{e}}_2\cdot\hat{\mathbf{r}}$$

After having expressed k_i^{mn} in terms of integrals of the dcf and isotropic tensors, one now employs the MSA for $c(1,2)$. We perform the integrals over $\mathbf{r}$, $\hat{\mathbf{e}}_1$, and $\hat{\mathbf{e}}_2$ in stages. First we employ the MSA for $c(1,2)$ so that eq 11 becomes

$$C_{jkm}^{\prime} = (4\pi)^{-2}\int d\Omega_1\, d\Omega_2 \left[-\rho^\circ\int_0^{HC} d\mathbf{r} + \beta\epsilon\int_{HC}^{SW} d\mathbf{r}\right] r^2(j,k,m) \tag{13}$$

where ρ° is given by eq 6b. Integration of eq 13 is to be taken over the hard core (0 to HC) and from the hard core boundary (HC) to the spherical square well outer lip (SW). The square-well integral can be written as the difference in two integrals ($\int_0^{SW} - \int_0^{HC}$), and when this result is inserted in eq 13, we obtain

$$C_{jkm}^{\prime} = -(4\pi)^{-2}\int d\Omega_1\, d\Omega_2 \left[(\rho^\circ + \beta\epsilon)\int_0^{HC} d\mathbf{r} - \beta\epsilon\int_0^{SW} d\mathbf{r}\right] r^2(j,k,m) \tag{14}$$

When the square-well portion ($\int_0^{SW}$) of eq 14 is integrated over a spherical domain, the anisotropic (j,m,n) functions vanish, so that

$$C_{jkm}^{\prime} = -(4\pi)^{-2}(\rho^\circ + \beta\epsilon)\int d\Omega_1\, d\Omega_2 \int_0^{HC} d\mathbf{r}\, r^2(j,k,m) \tag{15}$$

Each expansion coefficient requires an integration over the hard core and contains density and temperature as mere multiplicative factors. Thus all the geometric features of this model are determined by the HC alone.

The $\mathbf{r}$ integration, inside the excluded volume of the hard core, is performed by a scaling procedure. As discussed previously,[10] one transforms the integration variables from $\mathbf{r}$ to $\lambda\mathbf{R}(\mathbf{k})$ where λ is the scaling variable which ranges from 0 to 1. $\hat{\mathbf{R}}(\mathbf{k})$, the center-to-center vector on the excluded volume surface, is a function of the surface normal, $\mathbf{k}(\theta,\phi)$, and the orientations of the two bodies. It follows that

$$d\mathbf{r} = \lambda^2\, d\lambda\, d\hat{\mathbf{k}}\, S^{12}(\hat{\mathbf{k}},\hat{\mathbf{e}}_1,\hat{\mathbf{e}}_2)\, h_{12}(\hat{\mathbf{k}},\hat{\mathbf{e}}_1,\hat{\mathbf{e}}_2) \tag{16a}$$

S^{12} is the surface area per unit solid angle for the excluded volume surface:

$$S^{12} \equiv S^{12}(\hat{\mathbf{k}},\hat{\mathbf{e}}_1,\hat{\mathbf{e}}_2) = |(\partial\mathbf{R}/\partial\theta)\times(\partial\mathbf{R}/\partial\phi)\cdot\hat{\mathbf{k}}|_{\hat{\mathbf{e}}_1,\hat{\mathbf{e}}_2}/\sin\theta \tag{16b}$$

and h_{12} is the support function for the pair of bodies:

$$h_{12} \equiv h_{12}(\hat{\mathbf{k}},\hat{\mathbf{e}}_1,\hat{\mathbf{e}}_2) = \hat{\mathbf{k}}\cdot\mathbf{R} \tag{16c}$$

Both S^{12} and h_{12} are given explicitly elsewhere.[24] By means of eqs 16a–c and the scaling relation between $\mathbf{r}$ and $\mathbf{R}$, one can now write

$$C_{jkm}^{\prime} = {}^4/_5\pi(\rho^\circ + \beta\epsilon)\langle R^2\rangle_{jkm} \tag{17a}$$

with

$$\langle R^2\rangle_{jkm} = -(4\pi)^{-2}\int d\Omega_1\, d\Omega_2\, (j,k,m)R^2S^{12}h_{12} \tag{17b}$$

where we have integrated over the scaling variable ($\int_0^1 d\lambda\,\lambda^4$) and have used the result that $\mathbf{k}$ itself can be isotropically distributed (hence $\int d\hat{\mathbf{k}} = 4\pi$).

By means of eq 17 we can express k^{22} and k^{42} as

$$k_{[1,2,3]}^{22} = (4\pi/5)(\rho^\circ + \beta\epsilon)\{{}^5/_2\langle R^2\rangle_{220} + (1/14)^{1/2}[-1,2,-1]\langle R^2\rangle_{222}\} \tag{18a}$$

$$k_{[1,2,3]}^{42} = (4\pi/5)(\rho^\circ + \beta\epsilon)\{{}^{45}/_{16}\langle R^2\rangle_{440} + (5/56)^{1/2}[-3,-1,4]\langle R^2\rangle_{422}\} \tag{18b}$$

The $\langle R^2\rangle_{jkm}$ terms contain no density or temperature dependence and are determined completely by the geometry of the hard core. This suggests that one separate in the expression for K_i the thermodynamic properties from the purely steric properties:

$$K_i = (4\pi/5)\rho^2 k_B T(\rho^\circ + \beta\epsilon)\{\langle P_2\rangle^2\alpha_i^{22} + 2\langle P_2\rangle\langle P_4\rangle\alpha_i^{24}\} \tag{19}$$

Here $\{\alpha\}$ contain the steric information and are

$$\alpha_{[1,2,3]}^{22} = {}^5/_2\langle R^2\rangle_{220} + (1/14)^{1/2}[-1,2,-1]\langle R^2\rangle_{222} \tag{20a}$$

$$\alpha_{[1,2,3]}^{42} = {}^{45}/_{16}\langle R^2\rangle_{440} + (5/56)^{1/2}[-3,-1,4]\langle R^2\rangle_{422} \tag{20b}$$

When the molecules are biaxial (although the nematic phase is uniaxial), cross terms between the primary order parameter $\langle P_2\rangle$ and the biaxial order parameter $\langle F_2\rangle$ arise in eq 19. However, the coefficient of the $\langle P_2\rangle\langle F_2\rangle$ cross term is small, and so eq 19 provides an estimate of the Frank constants for biaxial bodies, provided of course that the integrations are performed over the biaxial excluded volume surface. The procedures required for this are discussed elsewhere.[25]

(21) de Jeu, W. H. *Physical Properties of Liquid Crystalline Materials*; Gordon and Breach: New York, 1980.
(22) Priest, R. G. *Phys. Rev.* **1973**, *A7*, 720.
(23) Straley, J. P. *Phys. Rev.* **1973**, *A8*, 2181.
(24) Talbot, J.; Kivelson, D.; Allen, M. P.; Evans, G. T.; Frenkel, D. *J. Chem. Phys.* **1990**, *92*, 3048.
(25) Tjipto-Margo, B.; Evans, G. T. *J. Chem. Phys.* **1991**, *94*, 4546.

(4) Computer Simulations. Simulation values of the elastic constants were obtained by molecular dynamics (MD), although Monte Carlo calculations would have been equally satisfactory as these are static quantities. The technical details have been given elsewhere,[26,27] so we briefly summarize the method here.

Collision-by-collision MD simulations were carried out for 3:1:1, 5:1:1, and 10:1:1 prolate hard ellipsoids and for 5:5:1 and 10:10:1 oblate hard ellipsoids. For the 3:1:1 we used a system size of 144 particles, in cuboidal periodic boundaries; for the other cases we employed truncated octahedral periodic boundary conditions and system sizes of 216 (5:1:1 and 5:5:1) and 500 (10:1:1 and 10:10:1). Typical production run lengths were (0.5–1.6) × 10^6 collisions, depending on the density: thus the results were averaged over times $t_{run} \simeq 2000$–$15000t_c$, where t_c is the mean time between collisions per molecule.

To calculate the elastic constants, we use Forster's expressions[28] in the form

$$\langle Q_{xz}(\mathbf{q})\, Q_{xz}(-\mathbf{q})\rangle = {}^9/_4\langle P_2\rangle^2 V k_B T/(K_1 q_x^2 + K_3 q_z^2) \quad (21a)$$

$$\langle Q_{yz}(\mathbf{q})\, Q_{yz}(-\mathbf{q})\rangle = {}^9/_4\langle P_2\rangle^2 V k_B T/(K_2 q_x^2 + K_3 q_z^2) \quad (21b)$$

As before, we take the director to lie in the z direction. These expressions are valid at low q, q being the magnitude of the wave vector $\mathbf{q}$ which we take to lie in the xz plane. The quantity $\mathbf{Q}$ is the Fourier transform of the orientation density:

$$\mathbf{Q}(\mathbf{q}) = (V/N)\sum_i {}^3/_2(\mathbf{e}_i\mathbf{e}_i - {}^1/_3\mathbf{I}) \exp(i\mathbf{q}\cdot\mathbf{r}_i) \quad (22)$$

where $\mathbf{I}$ is the unit tensor.

We adopt the above equations, rather than eq 1 because of the difficulty of determining the direct correlation function from a simulation. The values of K_i obtained either way are equivalent: both sets of expressions are derived from the same free energy density. In practice, the K_i are obtained by rewriting eqs 21 as

$$E_{xz} = 9\langle P_2\rangle^2 V k_B T/(4k^2\langle Q_{xz}(\mathbf{q})\, Q_{xz}(-\mathbf{q})\rangle) = {}^1/_2(K_1 + K_3) + {}^1/_2(K_1 - K_3)\delta \quad (23a)$$

$$E_{yz} = 9\langle P_2\rangle^2 V k_B T/(4k^2\langle Q_{yz}(\mathbf{q})\, Q_{yz}(-\mathbf{q})\rangle) = {}^1/_2(K_2 + K_3) + {}^1/_2(K_2 - K_3)\delta \quad (23b)$$

where $\delta = (q_x^2 - q_z^2)/q^2$. Then simultaneous double polynomial fits in δ and q^2 are carried out for E_{xz} and E_{yz}, allowing the elastic constants to be extracted from the low-order coefficients. Some curvature is seen in the plots of E_{xz} and E_{yz} against δ and q^2, indicating that higher-q terms are not negligible at the values of q imposed by the simulation box, but the limiting slopes and intercepts are well defined. However the combination of curvature effects and simulation statistics allows us to place no higher precision on the results than ±10–15%.

III. Results

Frank constants were calculated theoretically by several ways: the Poniewierski–Stecki expression, eq 1; by the Gelbart–Ben-Shaul method;[7] and by a perturbation theory approach, eq 19, initially suggested by Priest[22] and Straley.[23] Furthermore, the Frank constants were determined numerically from simulations.

The Poniewierski–Stecki and Gelbart–Ben-Shaul methods are equivalent. The advantage of eq 1 is that the orientational distribution functions for particles 1 and 2 enter as derivatives of the orientational variable, so that the order parameter dependence of the Frank constants is manifestly quadratic. For simplicity we chose the Poniewerski–Stecki method. As for the perturbation scheme, matters are simpler still. The averages are performed over an isotropic fluid and hence have fewer degrees of freedom to integrate than those from eq 1. Furthermore, the perturbation method provides results which suggest a separation of the temperature and density dependence from the purely steric parts. The direct numerical integrations of eq 1 on the other hand provide more accurate results than do eq 19. Our first task is to determine under what circumstances do the perturbation expressions accurately represent the Frank constants.

Listed in Table I are the Frank constants for 3:1:1, 5:1:1, and 10:1:1 prolate hard ellipsoids and 3:3:1, 5:5:1, and 10:10:1 oblate hard ellipsoids, all of which were calculated on the basis of eqs 1 and 19. As the particle shape anisotropy increases, so do the errors associated with the perturbation method: not an entirely unanticipated trend. The perturbation expressions, first introduced by Priest and Straley, provide good estimates for the systems with shape anisotropies characteristic of real nematogens. The utility of the perturbation scheme is not diminished in the case of the convex peg in a round hole potential, for here too the perturbation expressions provide accurate assessments (to within 20% for 5:1:1 bodies) of the Frank constants calculated on the basis of eq 1.

Having established the utility of the perturbation expressions, various relations then follow. Listed in Table II are the values of $\langle R^2\rangle_{jkm}$, i.e., temperature independent measures of the nonsphericity of the dcf for prolate and oblate ellipsoids. Two properties emerge from the results in Table II. First, that $\langle R^2\rangle_{220}$ is much greater than $\langle R^2\rangle_{440}$, to the extent that the latter can be ignored; and second, that $\langle R^2\rangle_{222}$ and $\langle R^2\rangle_{422}$ are of opposite signs for prolate and oblate bodies. The result of the latter is that the inequality of prolate bodies $K_3 > K_1 > K_2$ is reversed for oblate bodies $K_2 > K_1 > K_3$. Both inequalities have been confirmed by experiment[29–31] and by other theories.[32,33]

In the limit of vanishing C_{440}, relations can be derived involving the Frank constants and the remaining three C coefficients. Consider the mean of the three Frank constants, K_{av}, and the difference of the bend (K_3) and splay (K_1) constants. By means of eqs 7 and 10, one has

$$\beta K_{av}/\rho^2 = {}^5/_2\langle P_2\rangle^2 C_{220} \quad (24a)$$

$$\beta(K_3 - K_1)/\rho^2 = (35/2)^{1/2}\langle P_2\rangle\langle P_4\rangle C_{422} \quad (24b)$$

As eqs 24a and 24b determine the C_{220} and C_{422} expansion coefficients and as C_{440} is negligible, K_2 can be used to determine the C_{222} part of the dcf. By measurement of the Frank constants, the fluid density, and the $\langle P_2\rangle$, $\langle P_4\rangle$ order parameters, one can measure the anisotropic expansion coefficients of $r^4c(1,2)$. These findings are independent of the model chosen to represent $c(1,2)$. Equation 24a will be used later in our work; eq 24b demonstrates that the sign of $K_3 - K_1$ is determined by the sign of the C_{422} expansion coefficient.

Generally the Frank constants (as shown in Table I) increase with fluid density. For prolate bodies, DFT values of K_3/K_1 increase more rapidly than the simulation values with similar behavior of K_1/K_3 for oblate bodies. Although the DFT and the simulation values of K_i exhibit similar trends, the simulation values exceed those from the Poniewierski–Stecki theory.

In Table III the Frank constants for 6:1:1 hard ellipsoids are contrasted with those of Poniewierski–Holyst (PH)[33] theory for spherocylinders (with length:width = 6:1). Differences arise between the present and the Poniewierski–Holyst representation of $c(r)$; nonetheless, both calculations give comparable order parameters and Frank constants, and the disagreement with the simulation results persists.

The calculation of the temperature dependence of K_i is facilitated by the use of the perturbation expression, eqs 18 and 19. This is particularly justified since for 3:1 particles there is merely

(26) Allen, M. P.; Frenkel, D.; Talbot, J. *Comput. Phys. Rep.* **1989**, *9*, 301.
(27) Allen, M. P.; Frenkel, D. *Phys. Rev.* **1988**, *A7*, 1813; **1990**, *A42*, 3641E.
(28) Forster, D. *Hydrodynamic Fluctuations; Broken Symmetry and Correlation Functions, Frontiers in Physics*; Benjamin: Reading, MA, 1975; Vol. 47.
(29) Gruler, H. *Z. Naturforsch.* **1973**, *28a*, 474.
(30) Warmerdam, T.; Frenkel, D.; Zijlstra, R. J. J. *J. Phys. (Paris)* **1987**, *48*, 319. Warmerdam, T.; Frenkel, D.; Zijlstra, R. J. J. *Liq. Cryst.* **1988**, *3*, 369. Warmerdam, T.; Nolte, R. J. M.; Drenth, W.; van Miltenburg, J. C.; Frenkel, D.; Zijlstra, R. J. J. *Liq. Cryst.* **1988**, *3*, 1087.
(31) Heppke, G.; Ranft, A.; Sabaschus, B. *Mol. Cyst. Liq. Crys. Lett.* **1991**, *8*, 17.
(32) Sokalski, K.; Ruijgrok, Th. W. *Physica* **1987**, *A113*, 126.
(33) Poniewierski, A.; Holyst, R. *Phys. Rev.* **1990**, *A41*, 6871.

TABLE I: Frank Constants for Prolate Ellipsoids: The Perturbation Method (Eqs 18 and 19), Direct Integration, and Simulation Values[a]

B:C:C elongation	ρ^*	$\langle P_2\rangle$	$\langle P_4\rangle$	perturbation K_1	perturbation K_2	perturbation K_3	direct integrations K_1	direct integrations K_2	direct integrations K_3	computer simulation $\langle P_2\rangle$	computer simulation $\langle P_4\rangle$	computer simulation K_1	computer simulation K_2	computer simulation K_3
3:1:1	0.555									0.7		0.45	0.41	1.5
	0.568	0.53	0.19	0.16	0.12	0.31	0.16	0.12	0.32					
	0.580	0.63	0.28	0.23	0.18	0.51	0.23	0.18	0.53					
	0.620	0.79	0.48	0.39	0.35	1.19	0.40	0.35	1.27					
	0.660	0.86	0.61	0.54	0.54	2.03	0.57	0.54	2.26					
	0.700	0.90	0.71	0.71	0.79	3.20	0.77	0.81	3.69					
5:1:1	0.370									0.28	0.06	0.06	0.06	0.12
	0.407	0.63	0.29	0.21	0.13	0.58	0.22	0.12	0.62	0.73	0.37	0.53	0.41	1.4
	0.444	0.78	0.48	0.33	0.23	1.34	0.36	0.21	1.52	0.82	0.52	0.99	0.76	2.4
	0.481	0.85	0.60	0.42	0.34	2.19	0.47	0.31	2.65	0.87	0.62	1.7	0.67	4.0
	0.520	0.89	0.69	0.51	0.46	3.30	0.59	0.43	4.23					
10:1:1	0.222									0.60	0.22	0.35	0.21	0.46
	0.248	0.71	0.39	0.23	0.13	0.96	0.30	0.11	1.17					
	0.259	0.76	0.46	0.26	0.16	1.29	0.36	0.13	1.65	0.80	0.49	0.55	0.39	2.1
	0.280	0.83	0.57	0.30	0.21	1.97	0.44	0.18	2.72					
	0.300	0.87	0.64	0.33	0.27	2.68	0.50	0.22	3.98					
	0.370	0.93	0.80	0.40	0.48	5.92	0.69	0.36	11.4	0.93	0.80	5.8	3.9	9.5
C:C:B elonation	ρ^*	$\langle P_2\rangle$	$\langle P_4\rangle$	perturbation K_1	perturbation K_2	perturbation K_3	direct integrations K_1	direct integrations K_2	direct integrations K_3	computer simulation $\langle P_2\rangle$	computer simulation $\langle P_4\rangle$	computer simulation K_1	computer simulation K_2	computer simulation K_3
3:3:1	0.568	0.53	0.19	0.35	0.68	0.20	0.35	0.69	0.19					
	0.580	0.63	0.28	0.56	1.06	0.29	0.57	1.08	0.28					
	0.620	0.79	0.48	1.27	2.23	0.50	1.33	2.37	0.47					
	0.660	0.86	0.61	2.13	3.60	0.70	2.33	3.96	0.66					
	0.700	0.90	0.71	3.32	5.46	0.94	3.76	6.21	0.88					
5:5:1	0.370									0.70	0.33	1.6	1.9	0.68
	0.407	0.63	0.29	0.64	1.26	0.30	0.66	1.32	0.27	0.78	0.43	3.1	3.3	0.77
	0.444	0.78	0.48	1.43	2.60	0.51	1.57	2.92	0.45	0.85	0.57	5.3	6.0	1.2
	0.481	0.85	0.60	2.31	4.05	0.69	2.70	4.81	0.59	0.88	0.67	7.3	10.0	3.2
	0.520	0.89	0.69	3.44	5.87	0.89	4.27	7.36	0.73					
10:10:1	0.222									0.74	0.39	2.2	3.7	0.97
	0.248	0.71	0.39	1.10	2.17	0.44	1.29	2.40	0.41					
	0.259	0.76	0.46	1.46	2.81	0.54	1.76	3.26	0.48	0.83	0.55	4.5	6.4	0.97
	0.280	0.83	0.57	2.21	4.08	0.71	2.80	5.09	0.59					
	0.300	0.87	0.64	2.98	5.38	0.86	3.99	7.15	0.68					
	0.370	0.93	0.80	6.48	11.2	1.51	10.3	17.8	0.98	0.94	0.81	27	31	5.2

[a] $\rho^* = \rho v_0$; K_i in k_BT/C; $v_0 = (4\pi/3)BC^2$.

TABLE II: Variation of $\langle R^2\rangle_{jkm}$ with Shape Anisotropy for Hard Ellipsoids[a]

elongation	$\langle R^2\rangle^*_{220}$	$\langle R^2\rangle^*_{440}$	$\langle R^2\rangle^*_{222}$	$\langle R^2\rangle^*_{422}$
3:1:1	0.537	0.026	−0.740	0.704
4:1:1	1.87	0.87	−3.45	2.91
5:1:1	4.79	0.37	−10.05	8.17
10:1:1	76.6	7.5	−187.2	154.6
3:3:1	0.0138	0.0007	0.0405	−0.0083
4:4:1	0.0166	0.0011	0.0522	−0.0106
5:5:1	0.0183	0.0014	0.0599	−0.0120
10:10:1	0.0213	0.0022	0.0762	−0.0139

[a] The $\langle R^2\rangle_{jkm}$ are reduced by a factor of $(2C)^5$, and the particle volume is $4\pi BC^2/3$.

a 5% underestimate of the results from the direct integration, eq 1, with those of the perturbation scheme. To compare our results for the "convex peg in a round hole potential" with experimental results on a prolate body (PAA),[29] we must first construct the phase diagram at 1 atm. Parameters required for the convex peg model representation of PAA include the following: (i) the particle volume, which was taken[34] to be 230 Å^3; (ii) the square-well radius

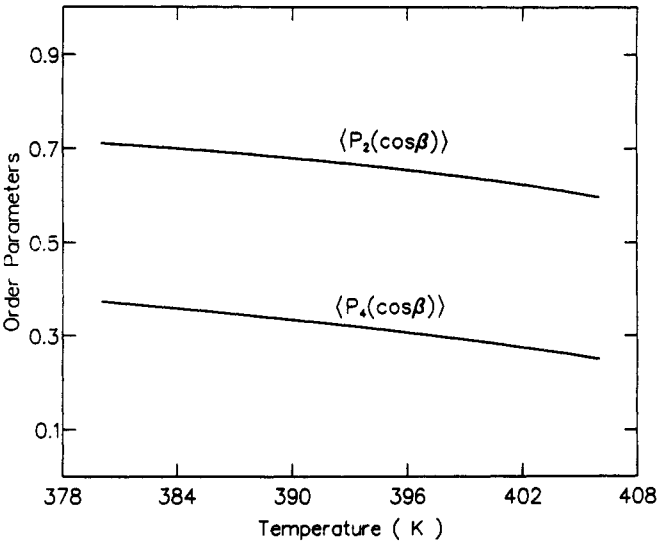

Figure 2. Variation of the order parameters with temperature for the convex peg model for a 3:1:1 prolate body resembling PAA.

TABLE III: Comparison of Frank Constants Derived by the PH Theory for Spherocylinders with the Present Theory for Ellipsoids with a Comparable Geometry[a]

B/C = 6 direct integrations ρ^*	$\langle P_2\rangle$	$\langle P_4\rangle$	K_1	K_2	K_3	L/D = 5 Holyst $\langle P_2\rangle$	K_1	K_2	K_3	MC ρ^*	$\langle P_2\rangle$	K_1	K_2	K_3
0.370	0.71	0.39	0.28	0.14	1.05	0.728	0.256	0.119	0.763	0.37	0.73	0.415	0.295	0.55
0.421	0.85	0.59	0.45	0.26	2.70	0.849	0.453	0.215	1.852	0.421	0.91	2.32	1.12	0.75

[a] Here the K_i are given in units of k_BT/C. For ellipsoids, C is the semiaxis length of the doubly degenerate axis; for spherocylinders, C is one-half the cap diameter.

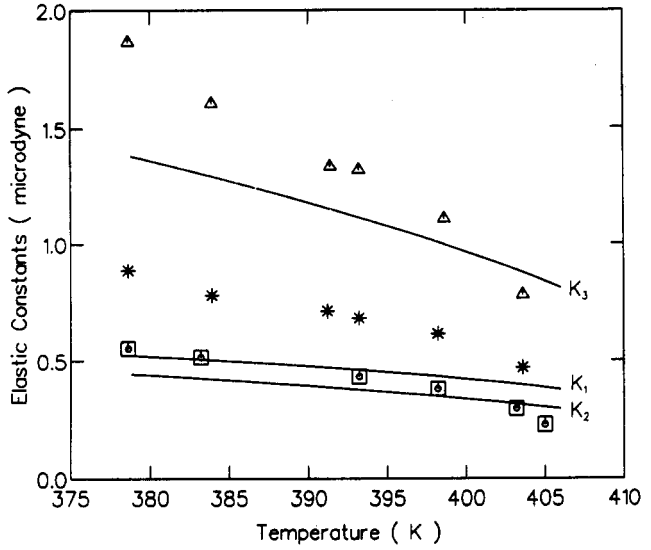

Figure 3. Theoretical and experimental[29] Frank constants for PAA. For both the experimental and theoretical results, $K_3 > K_2 > K_1$ (1 μdyn = 10^{-11} N).

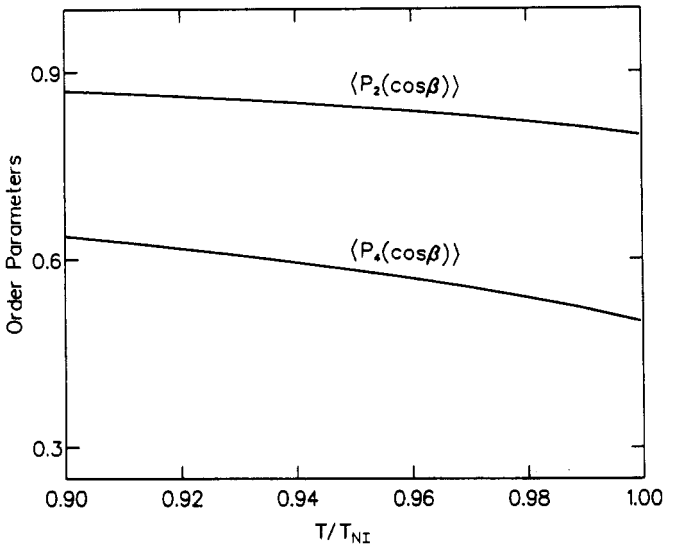

Figure 4. Temperature dependence of the order parameters for the convex peg model for a 4:4:1 oblate body representing B7.

(here taken to be twice the semimajor axis of the ellipsoidal core); (iii) the well depth of 427.7 K (derived by a fit of the pressure of 1 atm to a transition temperature of 407.7 K). From the temperature dependence of the calculated $\langle P_2 \rangle$ (shown in Figure 2) and from the calculated liquid-crystal density, we determine the elastic constants by means of eqs 19 and 20, and the results are shown in Figure 3. The agreement between the present results and the experimental PAA results in very good, especially in light of the Frank constants being unbounded quantities and the absence of adjustable parameters in our theory: an encouraging result indeed.

The Frank constants have also been measured[30,31] for oblate molecules (called B7, B8, and B9 in ref 31). For the B7 molecule, a 4:4:1 oblate geometry was chosen (based on elementary stereochemical considerations) with an accompanying molecular volume of 4290 Å^3. As before, the well depth (of 715.1 K) was derived by requiring the pressure to be 1 atm at a temperature of 402.2 K. With this information, the phase diagram was determined along with the temperature dependence of the order parameter, as shown in Figure 4. When we use these results together with the nematic densities, we obtain the elastic constants

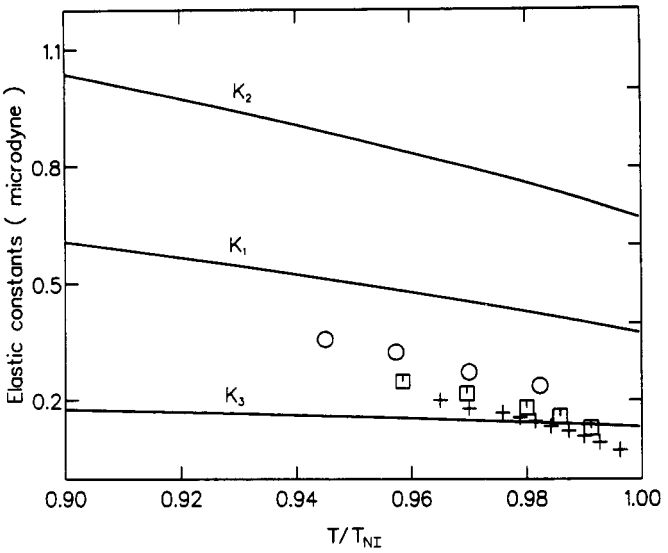

Figure 5. Theoretical convex peg model and experimental Frank constants[31] for B7 (○), B8 (□) and B9 (+).

of Figure 5. Although the agreement of the present theory with experiment is good for K_3, it is not nearly as good for K_1/K_3, as theory predicts this ratio to be roughly 2.8–3.4 whereas experimental values for B7, B8, and B9 vary from 1.1 to 1.5. In contrast, Warmerdam et al.[30] found that for slightly different discotic molecules (with roughly similar 4:4:1 geometries) K_1/K_3 ranged from 2.8 to 4.5, and this is in agreement with the present theoretical predictions.

Most nematogens are biaxial particles, and molecular biaxiality has a strong effect in decreasing the order parameters from their uniaxial analogues.[25] When the elastic constants for PAA were calculated using a biaxial convex peg potential (with a 3:1.4:1 geometry and a well depth of 738 K), K_i drop by a factor of 3 from their uniaxial values. Here we have assumed that the cross term between the uniaxial and biaxial order parameters, $\langle P_2 \rangle \langle F_2 \rangle$, is negligible since $\langle F_2 \rangle = 0.06$. This drop is attributable to both the decrease in $\langle P_2 \rangle$ from 0.6 for the uniaxial particle to 0.4 for the biaxial particle and to a secondary effect in that $\langle R^2 \rangle_{jkm}$ is smaller for biaxial particles than for uniaxials (since the biaxials are more spherical). As a consequence, had we used a more realistic biaxial geometry, such as that which fit the T dependence of the order parameter,[25] the present theory would underestimate the experimental results, just as theory underestimated the simulation results.

IV. Conclusions

The findings of this study are as follows: (i) Both the Poniewierski–Holyst work and the present work make similar predictions for K_i. (ii) The present calculations underestimate the simulation-derived Frank constants although not necessarily the Frank constant ratios. (iii) The present theory provides a good rendition of the experimental Frank constants, at the expense of using large order parameters. (iv) When a biaxial SW model with correct order parameters is used, the theoretically calculated Frank constants are too small.

One way to reconcile these findings is to note that the present model neglects long range correlations in $c(1,2)$. These same long-range correlations were of less importance for the calculation of the pressure and the phase diagram which samples integrals of the form $\int r^2 c(r)\, dr$,[18] but they become of increased importance for the Frank constants, which are proportional to integrals of the form $\int r^4 c(r)\, dr$.

To make this point more strongly, consider the ratio of the average Frank constant to the square of the order parameter as this ratio is related to a C_{220} (see eq 24a). When the experimental results for PAA (at 409 K) are compared with those for a 3:1:1 uniaxial body in a convex peg potential model, we find and

$$\{K_{av}/\langle P_2 \rangle^2\}_{exp}/\{K_{av}/\langle P_2 \rangle^2\}_{convex\ peg\ model} \approx 3$$

(34) Vieillard-Baron, J. *Mol. Phys.* **1974**, *28*, 809.

likewise, when we contrast the simulation results for a 3:1:1 uniaxial hard body with the present results, we obtain

$$\{K_{av}/\langle P_2\rangle^2\}_{simulation}/\{K_{av}/\langle P_2\rangle^2\}_{hard\ body\ model} \approx 2-3$$

which would suggest that the cause of the disagreement of theory with experiment (be it simulation or laboratory) arises not from anisotropic potential softness but rather from the long-range correlations missing in the present theory of $c(1,2)$. Whether the neglected long-range correlations arise from the approximation of $c(1,2;nem)$ by $c(1,2;isotropic)$ in the density functional theory or whether it be a case of better approximating the long-range correlations already present in the $c(1,2;isotropic)$, we cannot say. Further analysis of $c(1,2)$ for fluids of rods is necessary.

Acknowledgment. This paper was submitted in behalf of Marshall Fixman, as a way to express gratitude for his lasting influence on the scientific direction of G.T.E. The work presented here was supported in part by the US National Science Foundation, the NATO Foundation, and the Science and Engineering Research Council. The work of the FOM Institute is part of the research program of the FOM (Foundation for Fundamental Research of Matter) and is supported by the Dutch Organization for Scientific Research (NWO). B.T.-M. and G.T.E. are grateful to the hospitality of Professor John Rowlinson and Dr. Paul Madden of the Physical Chemistry Laboratory of Oxford University, where this work was begun. We also wish to express our indebtedness to Dr. Andrew J. Masters for several discussions of the issues presented here.

Light-Scattering Method of Determining the Second Virial Coefficient for Simple Molecules and Oligomers†

Yoshiyuki Einaga, Fumiaki Abe, and Hiromi Yamakawa*

Department of Polymer Chemistry, Kyoto University, Kyoto 606-01, Japan *(Received: September 10, 1991)*

A procedure of determining the molecular weight and second virial coefficient for simple molecules and oligomers from light-scattering measurements on a binary solution is presented on the basis of the well-established theory of fluctuations in multicomponent systems. It consists of determining first the total isotropic scattering from the solution and then the composition scattering by subtracting from the former the density scattering (the Einstein–Smoluchowski term), where the values at finite concentrations should be used for the density scattering and also for the refractive index and its increment appearing in the optical constant. The required value of the density scattering is obtained by multiplying its observed value for the pure solvent by the concentration correction factor that is evaluated from a proper relationship between the refractive index and density of the solution. From experimental results obtained for a solution of toluene in cyclohexane at 25.0 °C as an example, the Lorentz–Lorenz equation is recommended as such a relationship. It is demonstrated that the multiple scattering theory by Bullough, which has often been used, is erroneous.

I. Introduction

Recently we initiated a systematic experimental study of equilibrium conformational and steady-state transport properties of flexible polymers in dilute solutions in the unperturbed (Θ) state, using well-characterized samples over a wide range of molecular weight, including the oligomer region.[1,2] The data obtained have been analyzed on the basis of the helical wormlike chain model[3,4] with a consistent determination of the model parameters for individual polymers. As a next step, we are now planning to make a similar study of excluded-volume effects such as static and transport expansion factors and second virial coefficients, giving major attention to the oligomer region.

In the course of the above study, we have determined second virial coefficients A_2 from small-angle X-ray scattering measurements for atactic oligomers of styrene in cyclohexane at 34.5 °C (Θ)[5] and for those of methyl methacrylate in acetonitrile at 44.0 °C (Θ).[6] The results show that A_2 does not vanish but increases with decreasing molecular weight M, even at Θ (at which A_2 vanishes for very large M), in the range of M where the unperturbed mean-square radius of gyration is not proportional to M, i.e., in the oligomer region. A similar result was obtained also by Huber and Stockmayer,[7] who determined A_2 for the former system from light-scattering measurements. These findings indicate that the so-called two-parameter theory breaks down in the oligomer region, as is natural. However, a quantitative discussion should be based on a correct and accurate determination of A_2. For this purpose, light-scattering measurements are preferable, but then measurements must be carried out on generally optically anisotropic and rather concentrated solutions of oligomers. The object of the present paper is to resolve several problems that are then encountered, especially in the case of oligomers with small M or simple molecules.

We must first obtain the Rayleigh ratio $R_{\theta=0}$ due to the isotropic scattering at vanishing scattering angle θ from the total scattering intensity including the anisotropic contribution, but this step is rather straightforward. According to the theory of fluctuations in multicomponent systems,[8-10] we must then determine the component $\Delta R_{\theta=0}$ arising from concentration fluctuations (composition scattering) by subtracting from $R_{\theta=0}$ the component R_d (the Einstein–Smoluchowski term) arising from density fluctuations (density scattering) at *finite* concentrations. This is the most difficult step. Indeed, with an ingenious device, Coumou and co-workers[11,12] have measured directly the derivative $(\partial n/\partial p)_{T,m}$

† This paper is contributed to the celebration of the 60th birthday of Professor Marshall Fixman in recognition of his lasting contributions to theoretical polymer science.

(1) Konishi, T.; Yoshizaki, T.; Yamakawa, H. *Polym. J.* **1988**, *20*, 175.
(2) Konishi, T.; Yoshizaki, T.; Shimada, J.; Yamakawa, H. *Macromolecules* **1989**, *22*, 1921, and succeeding papers.
(3) Yamakawa, H. *Annu. Rev. Phys. Chem.* **1984**, *35*, 23.
(4) Yamakawa, H. In *Molecular Conformation and Dynamics of Macromolecules in Condensed Systems*; Nagasawa, M., Ed.; Elsevier: Amsterdam, 1988; p 21.
(5) Konishi, T.; Yoshizaki, T.; Saito, T.; Einaga, Y.; Yamakawa, H. *Macromolecules* **1990**, *23*, 290.
(6) Tamai, Y.; Konishi, T.; Einaga, Y.; Fujii, M.; Yamakawa, H. *Macromolecules* **1990**, *23*, 4067.
(7) Huber, K.; Stockmayer, W. H. *Macromolecules* **1987**, *20*, 1400.
(8) Kirkwood, J. G.; Goldberg, R. J. *J. Chem. Phys.* **1950**, *18*, 54.
(9) Stockmayer, W. H. *J. Chem. Phys.* **1950**, *18*, 58.
(10) See also: Yamakawa, H. *Modern Theory of Polymer Solutions*; Harper & Row: New York, 1971.

0022-3654/92/2096-3948$03.00/0 © 1992 American Chemical Society